



Monte Carlo modelling of pixel clusters in Timepix detectors using the MCNP code

Jaroslav Šolc ^{a,*}, Jan Jakubek ^b, Lukáš Marek ^b, Cristina Oancea ^b, Jiří Pivec ^b, Jana Šmoldasová ^a, Jiří Tesař ^a, Zdeněk Vykydal ^a

^a Czech Metrology Institute, Okružní 31, 638 00 Brno, Czech Republic

^b ADVACAM, U Pergamenky 12, 170 00 Prague 7, Czech Republic



ARTICLE INFO

Keywords:
Monte Carlo simulation
Pixel detector
UHDpulse
Charge sharing

ABSTRACT

The track structure of the signal measured by the semiconductor pixel detector Timepix3 was modelled in the Monte Carlo MCNP® code. A detailed model at the pixel-level (256 × 256 pixels, 55 × 55 μm^2 pixel size) was developed and used to generate and store clusters of adjacent hit pixels observed in the measured data because of particle energy deposition path, charge sharing, and drift processes. An analytical model of charge sharing effect and the detector energy resolution was applied to the simulated data. The method will help the user sort the measured clusters and distinguish radiation components of mixed fields by determining the response of Timepix3 detector to particular particle types, energies, and incidence angles that cannot be measured separately.

Introduction

In the planning and delivery of external radiation therapy with ionizing radiation (e.g., photons, electrons, protons), i.e. “radiotherapy”, the main focus placed on accurate delivery of the dose to the target volume and minimization of the dose to the surrounding critical organs. Currently, another topic of great interest in radiotherapy is the dosimetry outside the primary particle beam, or out-of-field dosimetry [1].

Out-of-field dose is caused by largely scattered primary radiation and by secondary radiation generated in interactions of primary beam with material. Mixed radiation fields are composed of particles of different type and energy, also called “stray radiation” or “scattered radiation”, and their composition heavily depends on the parameters of the primary beam, target material, and the distance from the beam axis. The stray radiation delivers extra dose to healthy tissue and critical organs outside the target volume. The dosimetry of mixed fields is challenged by the need of the identification of the field components.

The delivered amount of radiation to reach the therapeutic effect is expressed by absorbed dose, D_T , (in Gray, Gy). The result has a deterministic effect visible in a short period of time after irradiation, e.g., death or degeneration of a large number of cells at a time that may lead to the recovery from cancer. D_T is directly measurable by a dedicated instrument, e.g., ionization chamber. On the other hand, out-of-field

dosimetry is covered by radiological protection dosimetry because the radiation dose is much lower, in the region of stochastic effects below the threshold of deterministic effects. The equivalent dose in an organ or tissue, H_T (in Sievert, Sv), is used instead. This quantity is not directly measurable but is obtained from the D_T by applying radiation weighting factors, w_R , dependent on radiation type and energy, to reflect the relative biological effectiveness of the radiation [2]. This means that the determination of H_T requires the knowledge of the field composition.

In personalized dosimetry, the capability of measurement and proper identification of field components plays an important role in the risk assessment for various target categories of patients.

The development of traceable and validated methods for characterization of stray radiation is one of several goals of the joint European research project “Metrology for advanced radiotherapy using particle beams with ultra-high pulse dose rates” (18HLT04, UHDpulse) [34] aiming to develop a metrological framework for traceable absorbed dose measurements in ultra-high-dose-per-pulse (UHD) particle beams. It runs from 2019 to 2023 within the European Metrology Programme for Innovation and Research (EMPIR) organized by the European association of national metrology institutes EURAMET.

The project partner company ADVACAM, Czech Republic, aims to design, manufacture, test and validate an optimized pixel Timepix3-based detector for measurements of the absorbed dose from stray radiation fields generated by UHD beams [5] and its recalculation to the

* Corresponding author.

E-mail address: jsolc@cmi.cz (J. Šolc).

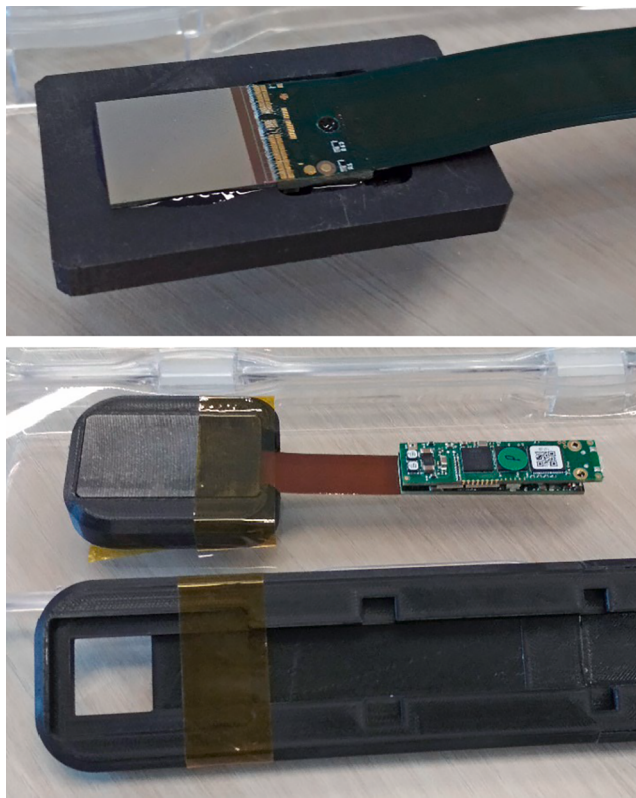


Fig. 1. Customized MiniPIX Timepix3 FLEX detector. Top: detail of Timepix3 chip assembly glued on extruded graphite cooling plate. Bottom: complete detector including readout electronics placed outside of its holder.

equivalent dose using the knowledge of the field composition. The development includes the work on methods to distinguish and characterize radiation components of mixed and time-dependent stray radiation fields occurring close to the UHD beam by the analysis of the measured signal. Due to the complexity of the task, Monte Carlo simulations were used in various steps of the work.

This paper describes the Monte Carlo modeling of the real track structure of the signal measured by the Timepix3 detector. The method includes an adaptation of an analytical model of charge sharing effect, which facilitates precise modelling of the so-called clusters of the adjacent hit pixels observed in the measured data caused by the particle path itself, charge sharing to adjacent pixels, and drift processes in the sensor material. The method will allow to optimize the sorting of measured clusters to distinguish radiation components by determining the response of the Timepix3 detector to the particular particle types, energies, and incidence angles, which cannot be measured separately.

Materials and methods

Timepix3 pixel detector

For the purpose of the dosimetry in mixed radiation fields generated by UHD beams, a specific customized version of MiniPIX Timepix3 Flex detector was developed (Fig. 1). The readout chip contains a matrix of 256×256 pixels (total 65 536 independent channels, pixel size $55 \mu\text{m}$) and an active sensor area of $14 \text{ mm} \times 14 \text{ mm}$ for a total sensitive area of 1.98 cm^2 [6]. This detector has the readout electronics detached from the Timepix3 ASIC and a sensor assembly to minimize scattering and self-shielding by using a 5-cm-long flexible printed circuit board [7]. Thanks to the timestamp of each hit with the precision of 1.5 ns and the energy absorbed in each individual pixel, the pixelized structure of the sensor allows recording of particle tracks. This version of the detector

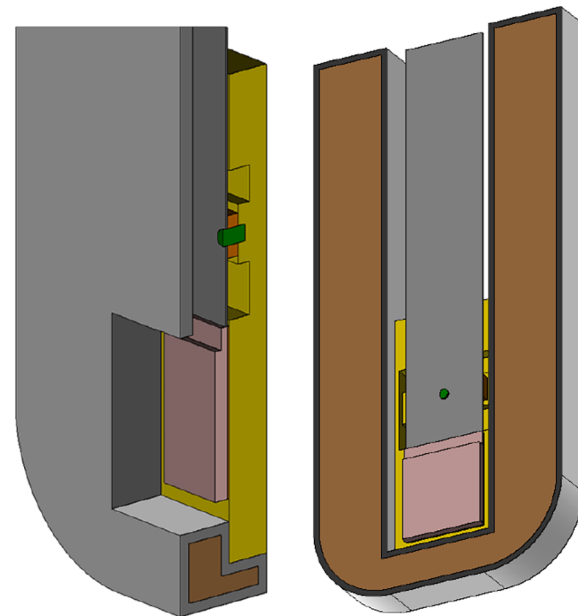


Fig. 2. Visualization of the MiniPIX Timepix3 FLEX Monte Carlo model. Colour indicates material: Si sensor and readout chip – ochre, graphite – yellow, PLA plastic (higher density) and flexible printed circuit board – grey, PLA plastic (lower density) – brown, steel – orange and green. (For interpretation of the references to colour in this figure legend, the reader is referred to the web version of this article.)

utilized the Si sensor 100 and $500 \mu\text{m}$ thick. The sensor was fully depleted as the high bias voltage was set to 50 V and 200 V, respectively. However, the pixel cluster modelling showed below was also tested for other sensors. If so, it is mentioned in the respective results section.

Particle tracking with Timepix-family detector is widely used and continuously improved, allowing up to 3D track mapping [8]. This paper deals with the standard 2D tracking with the emphasis on the charge sharing effect.

Monte Carlo modelling

Monte Carlo code

Monte Carlo (MC) simulations were performed with the code MCNP® in version 6.2 [9]. It is a general-purpose code for coupled ionizing radiation particle transport, developed in Los Alamos National Laboratory, USA. Specific areas of application include, but are not limited to, radiation protection and dosimetry [10], radiation shielding [11], medical physics [12], detector design and analysis [13], decommissioning [14], radiography, nuclear criticality safety, etc. Important standard features that make MCNP® very versatile and easy to use include a powerful general source, criticality source, and surface source, both geometry and output tally plotters, a rich collection of variance reduction techniques, a flexible tally structure, and an extensive collection of cross-section data. MCNP® contains numerous flexible tallies: surface current and flux, volume flux, point and ring detectors, particle heating, fission heating, pulse height tally for energy or charge deposition, mesh tallies, and radiography tallies [15].

The presented simulations used electron-photon relaxation library EPRDATA14 [16], electron library el03 [17], proton library ENDF/B-VII.0 [18], photonuclear reaction library ENDF/B-VII.0 [19], and neutron library ENDF/B-VIII.0 at 293.6 K [20]. Outside the energy range of libraries, the Bertini intranuclear cascade [21] with Dresner evaporation model [22] was used. Delayed particles from non-fission nuclear interactions were also considered.

The lower cut-off energy in the detection sensor was set as follows: 1 keV for electrons, 10 keV for photons, 300 keV for all other charged

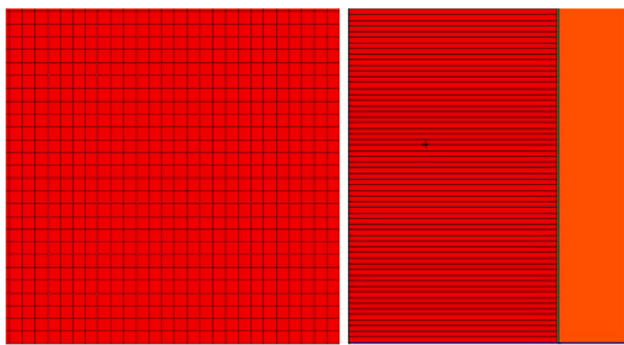


Fig. 3. Detail of pixelized structure of the MC model of Timepix3 detector. Left – top view, $55 \times 55 \mu\text{m}^2$ mesh; right – side view, $55 \times 2000 \mu\text{m}^2$ mesh. Pictures are not in scale to each other. Colour indicates material: red – sensor chip, orange – readout chip, green – bonding. (For interpretation of the references to colour in this figure legend, the reader is referred to the web version of this article.)

particles. Higher energy cut-off was set in materials surrounding the sensor to include the signal from particles created outside the sensor as well. No energy cut-off was set for neutrons. Generating of δ -electrons was turned off. Other parameters of particle physics on PHYS cards [9] were kept default.

No variance reduction methods were used because the weight of particles generating the signal in the sensor had to remain equal to one. Otherwise, the energy deposition and the ratio of different track types would be biased.

Timepix detector model

A detailed MC model of the MiniPIX Timepix3 FLEX device used in the UHDpulse project was developed comprising all parts relevant for ionizing particles transport (Fig. 2). Dimensions and material specification corresponded to the real device. The model included the sensor chip of the given material (Si, CdTe, or GaAs) and the thickness equal to the given sensor. The readout chip ($720 \mu\text{m}$ thick Si), glue ($250 \mu\text{m}$) and bonding ($20 \mu\text{m}$) of the sensor chip were also included. A graphite cooling plate below the readout chip, flex cables connecting the readout chip with electronics, and a 3D-printed holder and detector cover were modelled as well.

Particle tracks modelling

The goal was to model tracks of particles by means of scoring the deposited energy in each pixel of the sensor and to store all information for further data processing. To achieve this goal, a lattice (LAT card) was placed onto the whole sensor chip with $55 \times 55 \times Z \mu\text{m}^3$ mesh, where Z is the actual sensor chip thickness (Fig. 3) that varies depending on the detector expected application (typically between 100 and 2000 μm).

The particle track file (PTRAC card) was used to write and store information about the energy deposited in each pixel. The PTRAC card in simulation for mixed radiation field generated by UHD proton beam was set up as follows:

```
PTRAC FILE = ASC TYPE = P,E,H,A,D,T,S WRITE = ALL
EVENT = SRC SUR COL BNK TER
FILTER = 1,9,JSU 0,299,VEL
TALLY = 18 VALUE = 3E-3
```

Events written into the file included any particle crossing surfaces 1 to 9 (specifically reserved for lattice mesh and sensor chip borders only) and any interaction, generation, and termination event in the sensor that resulted in energy deposition higher than 3 keV by any charged particle. Photons were included to correctly count also electrons generated by photons originating in the sensor, e.g., characteristic and bremsstrahlung photons. The VEL parameter (limit on particle velocity) allowed to omit writing mesh surface crossings of photons into the PTRAC file and thus reduce its size. For simulations with primary particles of a different

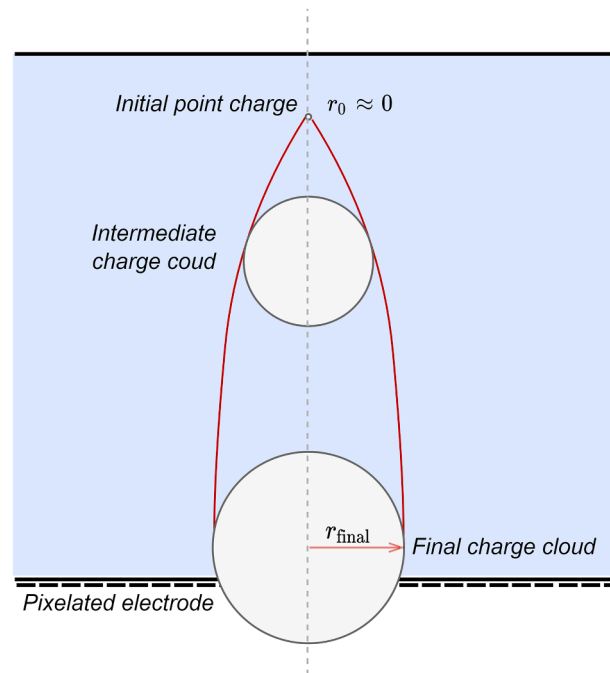


Fig. 4. Schematics of charge sharing effect. The initial charge cloud, considered point-like, evolves into a sphere cloud of radius r_{final} in the vicinity of the pixelated electrode.

type or different energy, the parameter TYPE was modified to match all particles that might occur in the detector. There is no information about particle track inside the pixel except for the information about particle termination or particle generation.

The parameters written in the PTRAC file relevant for data evaluation included particle type, event type, spatial coordinates of the event, direction vector, particle energy, and time.

Typically, 5×10^5 events were stored into the PTRAC file. The running time depended on the type of the source and the geometry.

MC data analysis

The PTRAC files generated by the MCNP® were processed in a purpose-written script in Matlab® software (The MathWorks®, USA). The individual steps of the analysis included:

- spatial coordinate transformation to the default coordinates of the software package Pixel Pro [23];
- calculation of a) energy deposited in each pixel and b) effective centre of the track in each pixel;
- application of the model of charge-sharing effect;
- application of the detector energy resolution.

The deposited energy in each pixel was calculated as the difference between the particle energy when entering the pixel (or particle initial energy if created there) and particle energy when leaving the pixel (if it crossed the sensor surface).

The effective centre of the track in each pixel was determined as the average X, Y, Z coordinates of particle location when entering the pixel (or location of particle origin if created there) and particle location when leaving the pixel (or location of particle end of path if terminated there).

Model of charge sharing effect

Charge sharing effect in pixel detectors indicates the sharing of initial charge cloud generated by ionizing particle between two or more adjacent pixels caused by the lateral spread of the cloud because of

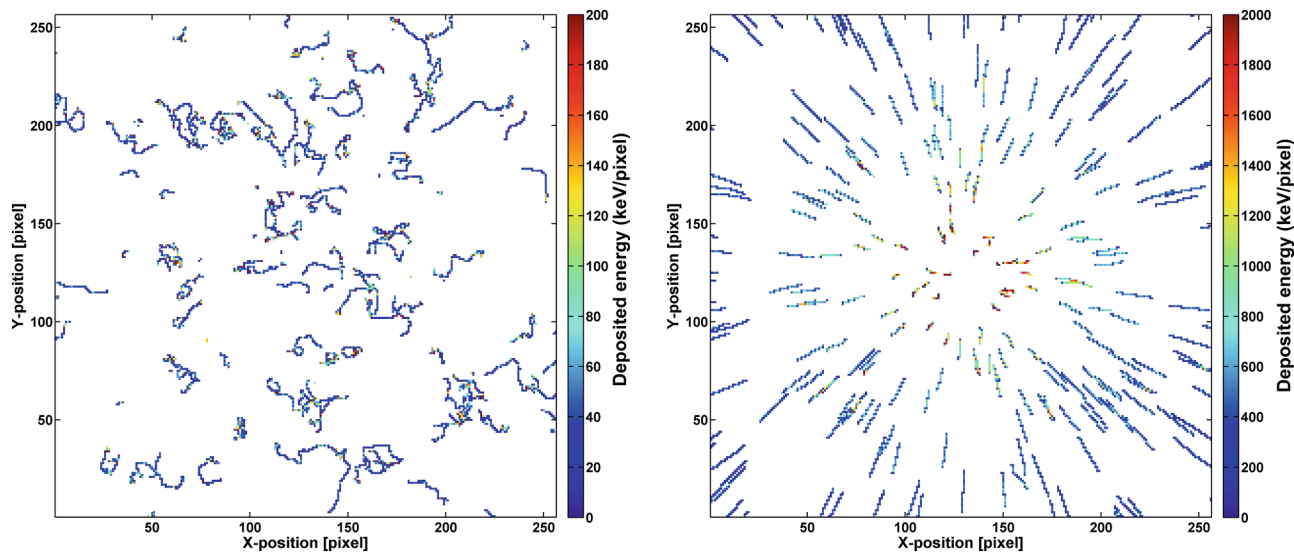


Fig. 5. Visualization of simulated clusters generated by 2.9 MeV electrons (left) and 50 MeV protons (right). Charge sharing not applied. Data for a Timepix3 detector with 2 mm thick CdTe sensor. See the text for the source specification.

electrical repulsion when traveling towards the read-out electronics accelerated by the electric field. The charge sharing in pixel detectors has been studied by many authors, e.g. [24–26]. The effect leads to the degradation of spatial and energy resolution of the detector [27] that is of high importance in medical applications where it causes reduction of dose efficiency [28] and image quality [29]. The charge sharing also affects the pixel detector energy calibration [30].

The analytical model of the expansion of the charge cloud generated in the sensor by ionizing radiation and the cloud's sharing between the adjacent pixels was developed (Fig. 4). It assumed the point generation of the initial charge. The model took into account electrical properties of the sensor material, bias voltage, depletion voltage, and the depth of particle interaction in the sensor.

The main principle relied on electric repulsion of the same charge within the charge cloud. The model assumed the initial charge distribution described by a Gaussian function with a certain known dispersion (potentially energy dependent). The model showed that the Coulomb repulsion dominated the charge sharing process especially for energies

larger than units of keV. The Coulomb repulsion dominates shortly (in a fraction of nanosecond) after the initial ionization and positive–negative charge separation. The charge distribution is shaped as homogeneous sphere with radius r :

$$r = \sqrt[3]{REt + C}$$

where R is material constant incorporating charge mobility and ionization energy for electron-hole production, E is energy of primary particle spent for ionization, t is charge collection time, and C is the initial charge size.

The charge diffusion is relevant in low energy range. The electrostatic induction in combination with charge sensitive preamplifier properties didn't contribute to the signal registered by pixels for deposited energy lower than about 1 MeV.

The model was applied on the simulated data. For each pixel with any energy deposition, the radius of the final charge cloud was calculated from the effective centre of the track. Then, the energy deposited at

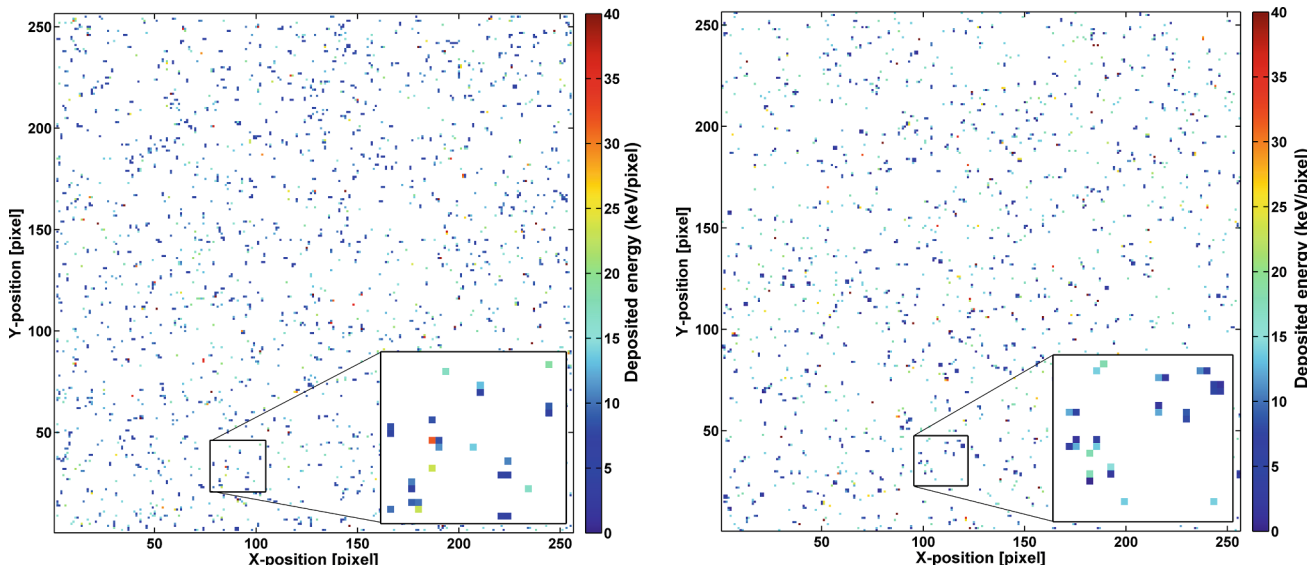


Fig. 6. Comparison between measured (above) and simulated (below; with charge sharing applied) pixel clusters from ^{241}Am radionuclide (main energies: gamma –60 keV, X-ray 12–22 keV). Data for a Timepix3 detector with 1 mm Si sensor.

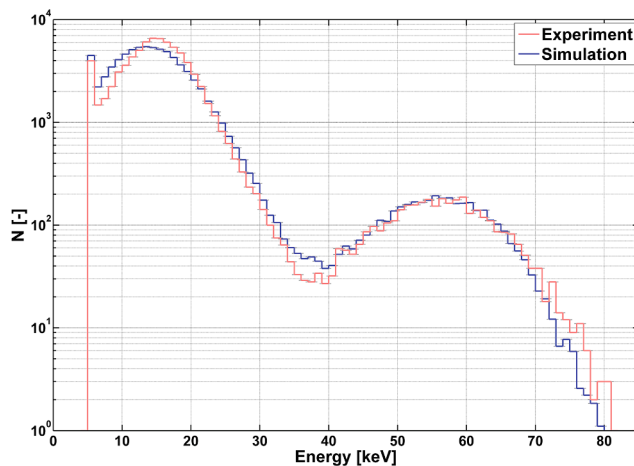


Fig. 7. Relative comparison between measured (red) and simulated (blue) energy spectrum of clusters for ^{241}Am photon source. Charge sharing and energy resolution were applied on simulated data. Data for a Timepix3 detector with 1 mm thick Si sensor. (For interpretation of the references to colour in this figure legend, the reader is referred to the web version of this article.)

a point in the simulation was spread over the final radius and recalculated into the pixels lying within this radius. The energy shared by each pixel due to the charge sharing effect was determined as the original total deposited energy multiplied by the relative volume of the charge cloud sphere in the given pixel. The relative volume was determined by random sampling of points inside the pixel and counting the hits inside the sphere, which proved to be the fastest method.

The energy resolution of the detector was applied on the simulated data after the charge sharing model had been employed. It describes the accuracy of the absorbed energy measurement and comprises the statistical noise, electronic noise, and operational drift components. The energy-dependent sensor-wise energy resolution function was measured out of the scope of this work for several Timepix3 detectors using selected suitable radionuclides emitting photons (X-ray fluorescence and γ) in the energy range from 14 keV to 662 keV. It was determined from the full-width-at-half-maximum of full-energy peaks in the measured energy spectra of clusters in the whole sensor area. The energy resolution was applied as follows: First, for each cluster, a random difference

from the true total deposited energy was determined by random number generation from Gaussian distribution using sigma (variation from the mean) taken from the energy-dependent energy resolution function for the given deposited energy and for the given sensor (material, thickness, settings). Then, the difference was split among all pixels of the given cluster linearly with respect to the energy in each pixel.

Results and discussion

Comparison of measured and simulated clusters in various fields

The method for pixel clusters modelling was initially tested on imaginary point isotropic sources of monoenergetic 50 MeV protons and 2.9 MeV electrons originating at the sensor normal at 1 cm distance from the sensor. Fig. 5 shows the visualization of particle tracks. Clusters created by protons are nearly straight and heading from the source. The cluster length increases with the increasing angle of the proton path from the sensor normal, intersecting more pixels. The electron tracks, on the contrary, are largely curved because of straggling at numerous interactions and therefore the direction to the source is not obvious. The clusters are not broken and their shape, neglecting charge sharing effects, corresponds with our experience.

The comparisons of simulated clusters and real measured clusters created in various particle fields are presented in Figs. 6–11. Fig. 6 shows the integral frames with clusters generated by photons from ^{241}Am quasi-point source in 1 mm thick Si sensor. The source was positioned in air at the distance of 10 cm from the detector on the sensor normal. Because of low energy of photons (<60 keV) and small radius of charge sharing, the clusters are typically composed of 1 to 3 pixels. Fig. 7 shows the comparison of the measured and simulated detector pulse-height spectra, where each pulse represents the sum of energy deposited in all pixels of one cluster. Energy resolution of the given detector was applied on the simulated data. A good agreement was achieved. One of the main sources of a minor discrepancy was caused by the energy calibration of the detector. It can be observed in the position of the main two peaks (~14 keV and 60 keV), which should be in the ideal case in accordance with the simulation.

A similar result is depicted in Fig. 8 for ^{137}Cs source. The experimental setup was the same as in the case of ^{241}Am source. Some clusters are longer because of higher maximum photon energy emitted by ^{137}Cs (662 keV) compared to ^{241}Am . In addition, the ^{137}Cs also emits beta radiation with the maximum energy of 1175 keV (5.6 % yield). Higher

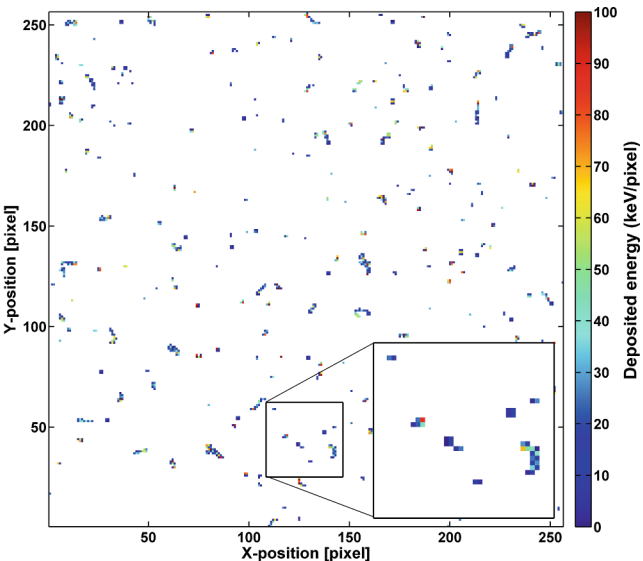
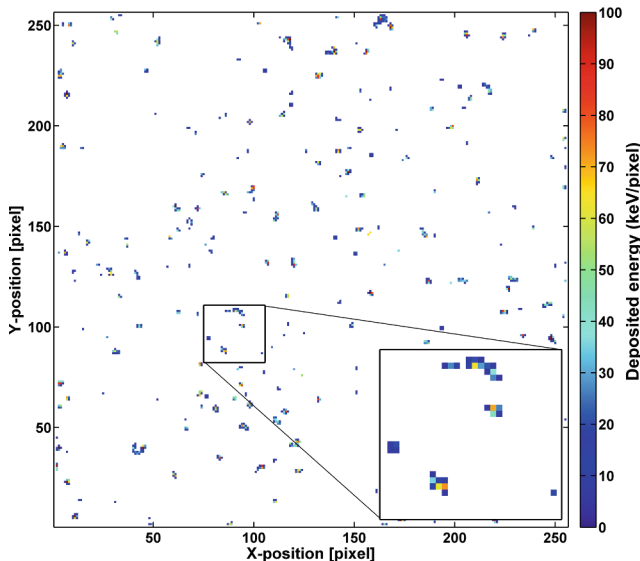


Fig. 8. Comparison between measured (above) and simulated (below; with charge sharing applied) pixel clusters from ^{137}Cs radionuclide (main energies: gamma – 662 keV, X-ray 32–37 keV). The beta radiation was included in simulated data. Data for a Timepix3 detector with 1 mm thick Si sensor.

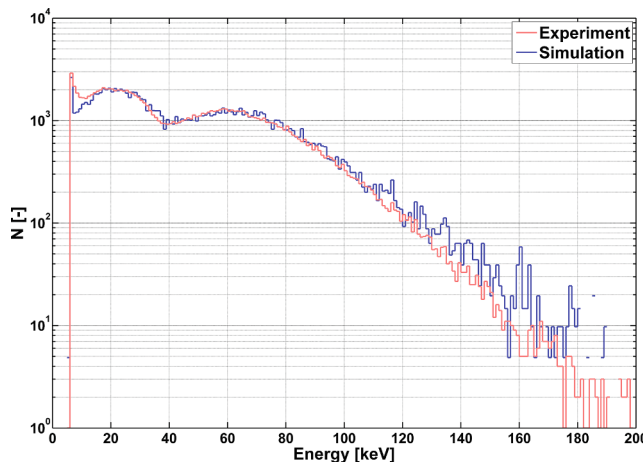


Fig. 9. Relative comparison between measured (red) and simulated (blue) spectrum of maximum deposited energy in a pixel in cluster for ^{137}Cs photon source. The charge sharing and energy resolution were applied on simulated data. Beta radiation was included in simulations. Results for Timepix3 detector with 1 mm thick Si sensor. (For interpretation of the references to colour in this figure legend, the reader is referred to the web version of this article.)

energy beta particles also reached the detector because there was no absorber: there was no detector input window and the 1.5 mm thick polystyrene cover of the point source did not completely absorb the electrons. Beta radiation was included in the simulation. Fig. 9 compares the measured and the simulated maximum deposited energy in a pixel in cluster.

Fig. 10 presents the comparison between the measured and the simulated clusters resulting from thermal neutrons. Neutron detection was possible using the Timepix3 detector equipped with suitable neutron convertors [31]. For thermal neutron detection, a convertor made from Lithium Fluoride enriched by ^6Li nuclide was used in a form of a thin (~10 μm) layer placed above a part of a sensor (~300 μm distance). In Fig. 10 the convertor used for measurements had an area of 50×250 pixels and was placed on the top part of the sensor ($Y = [246–256]$ and $X = [0–256]$ pixels). To enhance the sensitivity and impact of the neutron convertor, in this simulation the ^6LiF layer was located in the upper part of the sensor covering a larger area ($Y = [180–256]$ and $X = [0–256]$ pixels).

[180–256] and $X = [0–256]$ pixels).

Thermal neutrons interact with ^6Li creating triton and alpha particle ions. The ions are emitted in the direction heading away from each other and one of them usually reaches the detector and generates a thick circular cluster. Fig. 10 shows such tracks recognised as ions created by the thermal neutron interactions in the converter.

Thermal neutron detection efficiency strongly depends on the ^6LiF layer properties (thickness, distance, enrichment, homogeneity, glue concentration, etc.) and each piece of the converter is unique and has to be calibrated individually together with the given piece of the detector/sensor. That is why the parameters of MC model of the converter (thickness, distance, area) have to be always tuned to match the measured detection efficiency (number of clusters per cm^2 per unit fluence of thermal neutrons) of the given device/convertor. The presented results were obtained for 500 μm thick Si sensor with a converter providing the thermal neutron detection efficiency of about 1.6 % that is similar to the data presented in [31].

Fig. 11 shows the comparison between the measured and the simulated clusters created by 220 MeV proton beam delivered to a water phantom at a therapeutic proton therapy facility. Specifically, a complex mixed radiation field was measured and simulated on the beam axis about 4 cm behind the Bragg peak. The frames show a large number of different cluster types generated by various particles – thick circular and long tracks from recoiled protons, thin long tracks from high energy electrons, and short tracks from low energy electrons.

There was a noticeable difference in the shape of large circular clusters created by low energy ($E < \sim 10$ MeV) recoiled protons. Small amount of energy was registered also by pixels farther from the interaction point creating a corona effect caused by local distortion of electric field caused by a huge amount of charge generated at one place. Such effect was not observed in simulated clusters because this phenomenon was not described by the charge sharing model.

To provide accurate simulations of the clusters made by scattered particles to characterise the mixed radiation fields created in therapeutic proton and electron beams is the main goal of this work. In the case presented in Fig. 11, the radiation field was composed by primary protons, recoiled nuclei, secondary photons and neutrons generated in proton nuclear interactions, and tertiary charged particles generated by secondary photons and neutrons.

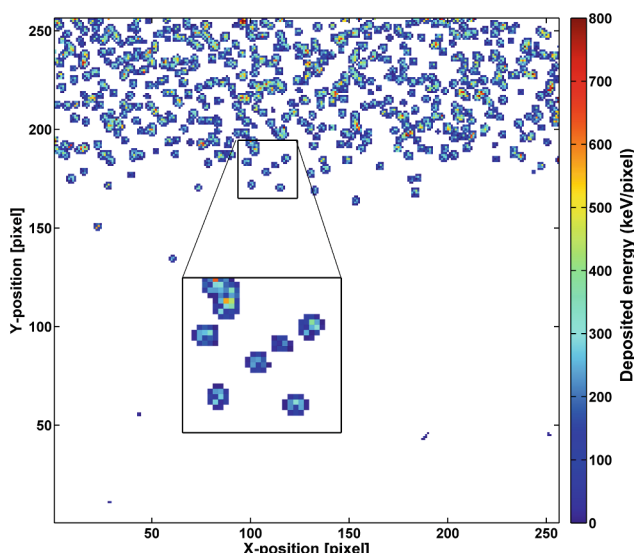
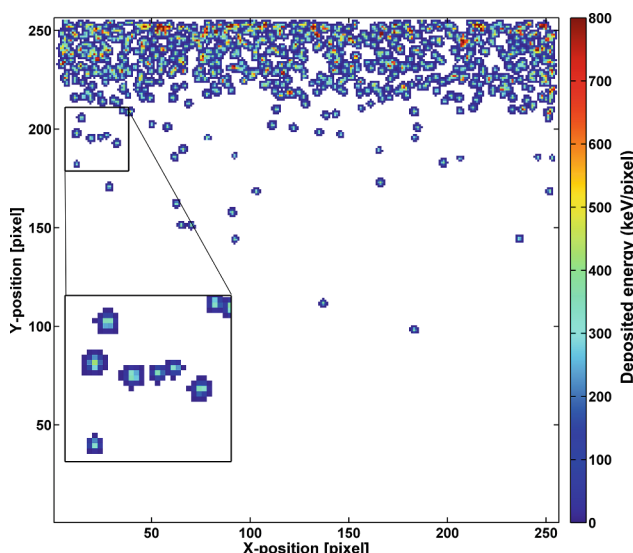


Fig. 10. Comparison between measured (above) and simulated (below; with charge sharing applied) clusters generated by tritons and alpha particles originating from ^6Li disintegration from interaction of thermal neutrons. The ^6LiF layer was placed over the top part of the sensor at the distance of about 300 μm . Different areas were covered in measurement and simulation. Data for a Timepix3 detector with 500 μm thick Si sensor.

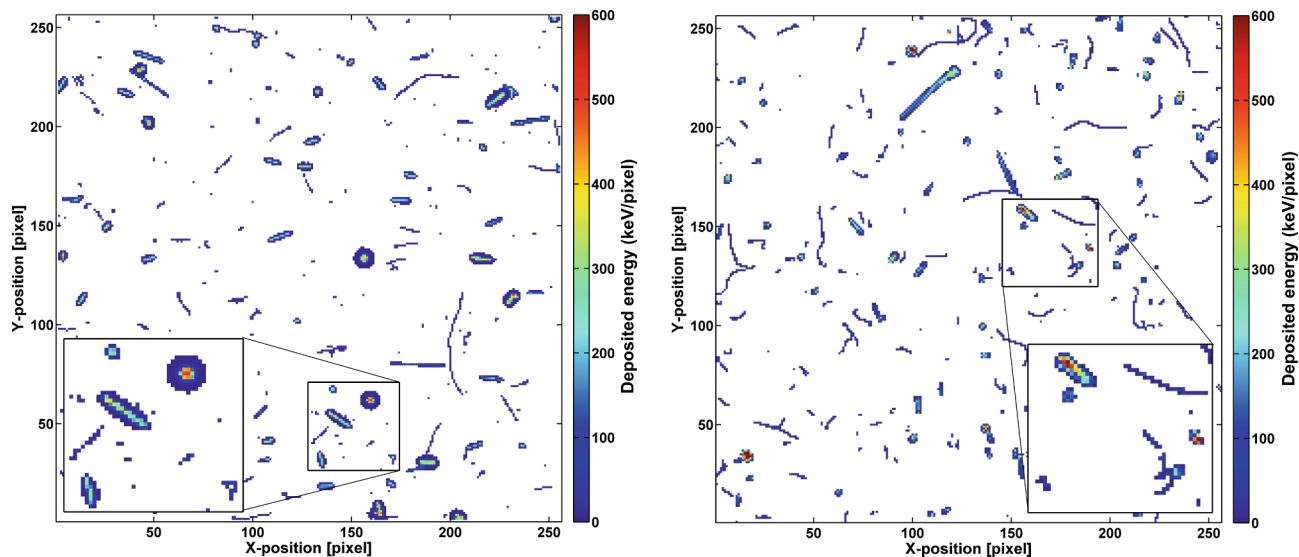


Fig. 11. Comparison between measured (above) and simulated (below; with charge sharing applied) clusters created in a detector immersed into a water phantom 4 cm behind the Bragg peak of 220 MeV monoenergetic protons. Data for a Timepix3 detector with 500 μm thick Si sensor.

The charge sharing model summary

The analytical model of charge sharing effect has recently been developed for point deposition of the charge, assuming the spherical expansion of the charge cloud based on the electric repulsion. That is applicable especially for low energy electrons ($E < \sim 50 \text{ keV}$). The model simplifies charge sharing a) for long tracks where the charge is generated continuously along the path of the charged particle, for example, high energy protons ($E > \sim 50 \text{ MeV}$) or electrons ($E > \sim 200 \text{ keV}$), and b) for very high energy depositions at one place, for example low energy protons ($E < \sim 10 \text{ MeV}$). The model can be improved also by including other physical effects, such as the charge diffusion, recombination, or the electrostatic induction.

However, the presented results are sufficient for the first approximation of the charge sharing effect in the Timepix-family semiconductor pixel detectors. The model will be further studied and improved in the next work.

Conclusions

In the MCNP radiation transport code, Monte Carlo model of MiniPIX Timepix3-FLEX pixel detector was developed. The model was voxelized into 256×256 pixels and allows simulating per-pixel deposited energy and storing the data for further analysis. A model of charge sharing between adjacent pixels was adapted for the use on simulated data to realistically simulate the shape of pixel clusters depending on the particle type, deposited energy, interaction depth, sensor parameters, and measurement settings. The method helps to optimize the sorting of measured clusters to distinguish radiation components especially in conditions where it is not possible to determine it experimentally. Ultimately, the developed method may improve the measurement of equivalent dose in mixed particle fields by Timepix3 detectors.

Declaration of Competing Interest

The authors declare that they have no known competing financial interests or personal relationships that could have appeared to influence the work reported in this paper.

Acknowledgements

This project 18HLT04 UHDpulse has received funding from the

EMPIR programme co-financed by the Participating States and from the European Union's Horizon 2020 research and innovation programme.

References

- [1] Kry SF, Bednarz B, Howell RM, Dauer L, Followill D, Klein E, et al. AAPM TG 158: Measurement and calculation of doses outside the treated volume from external-beam radiation therapy. *Med Phys* 2017;44:e391–429. <https://doi.org/10.1002/mp.12462>.
- [2] ICRP. 2010. Conversion Coefficients for Radiological Protection Quantities for External Radiation Exposures. ICRP Publication 116, Ann. ICRP 40(2-5).
- [3] Schüller A, Heinrich S, Fouillade C, Subiel A, De Marzi L, Romano F, et al. The European Joint Research Project UHDpulse – metrology for advanced radiotherapy using particle beams with ultra-high pulse dose rates. *Phys Med* 2020;80:134–50. <https://doi.org/10.1016/j.ejmp.2020.09.020>.
- [4] Project website: <http://uhdpulse-empir.eu/>. Accessed 21 June 2022.
- [5] Oancea C, Granja C, Marek L, Pivec J, Jakubek J, Šolc J, Bodensteind E, Gantzd S, Pawelke J. Characterization of scattered radiation in conventional and FLASH proton beam using a Timepix3 detector: Dose rate, Flux, and LET measurements, *Physica Medica*, FRPT2021 special issue, submitted.
- [6] Poikela T, Plosila J, Westerlund T, Campbell M, De Gaspari M, Llopard X, Gromov V, et al.. Timepix3: a 65 K channel hybrid pixel readout chip with simultaneous ToA/ToT and sparse readout, 2014 *JINST* 9 C05013. <https://doi.org/10.1088/1748-0221/9/05/C05013>.
- [7] Oancea C, Bălan C, Pivec J, Granja C, Jakubek J, Chvatil D, et al. Stray radiation produced in FLASH electron beams characterized by the MiniPIX Timepix3 Flex detector. *JINST* 2022;17:C01003. <https://doi.org/10.1088/1748-0221/17/01/C01003>.
- [8] Bergmann B, Burian P, Manek P, Pospisil S. 3D reconstruction of particle tracks in a 2 mm thick CdTe hybrid pixel detector. *Eur Phys J C* 2019;79:165. <https://doi.org/10.1140/epjc/s10052-019-6673-z>.
- [9] Werner Ch J. 2017. MCNP® User's Manual, Code Version 6.2, Los Alamos National Laboratory LA-UR-17-29981.
- [10] Kozlovska M, Šolc J, Otahal P. Measuring and Monte Carlo modelling of X-ray and gamma-ray attenuation in personal radiation shielding protective clothing. *Comput Math Methods Med* 2019;1–8. <https://doi.org/10.1155/2019/1641895>.
- [11] Šolc J, Kovar P, Suran J, Grisa T. Monte Carlo optimization of shielding for novel industrial free release measurement facility. *Appl Radiat Isot* 2017;126:73–5. <https://doi.org/10.1016/j.apradiso.2016.12.032>.
- [12] Králik M, Šolc J, Vondráček V, Smoldasová J, Farkašová E, Tichá I. Spectral fluence of neutrons generated by radiotherapeutic linacs. *Radiat Prot Dosim* 2015;163(3):373–80. <https://doi.org/10.1093/rpd/ncu192>.
- [13] Sochor V, Šolc J. Characterization of the new free-air primary standard for medium-energy X-rays at CMI. *JINST* 2018;13:P08008. <https://doi.org/10.1088/1748-0221/13/08/P08008>.
- [14] Šolc J, Kovar P, Suran J, Peyres V, Garcia-Torano E. Optimization of a measurement facility for radioactive waste free release by Monte Carlo simulation. *Appl Radiat Isot* 2014;87:348–52. <https://doi.org/10.1016/j.apradiso.2013.11.005>.
- [15] MCNP® code website: <https://mcnp.lanl.gov/>. Accessed 30 March 2022.
- [16] Werner Ch J, Bull J S, Solomon CJ, Brown FB, McKinney GW, Rising ME, Dixon DA, et al.. MCNP Version 6.2 Release Notes, Los Alamos National Laboratory LA-UR-18-20808, 2018.

- [17] Adams KJ. Electron Upgrade for MCNP4B, Los Alamos National Laboratory, X-5-RN(U)-00-14, 2000.
- [18] Trellue H, Little R, Lee M B. New ACE-Formatted Neutron and Proton Libraries Based on ENDF/B-VII.0, Los Alamos National Laboratory LA-UR-08-1999, 2008.
- [19] Chadwick M B, Oblozinský P, Herman M, Greene NM, McKnight RD, Smith DL, et al.. ENDF/B-VII.0: next generation evaluated nuclear data library for nuclear science and technology nuclear data sheets. 107, 2931–3060, 2006. <https://doi.org/10.1016/j.nds.2006.11.001>.
- [20] Conlin J L, Haeck W, Neudecker D, Parsons D K, White M C. Release of ENDF/B-VIII.0-Based ACE Data Files, Los Alamos National Laboratory LA-UR-18-24034, 2018.
- [21] Prael RE, Liechtenstein H. User Guide to LCS: the LAHET Code System. Los Alamos National Laboratory LA-UR-89-3014, 1989.
- [22] Dresner L. EVAP: A FORTRAN program for calculating the evaporation of various particles from excited compound nuclei. Oak Ridge National Laboratory ORNL-TM-196, USA, 1962. <https://doi.org/10.2172/4638868>.
- [23] Turecek D, Jakubek J. Software Pixet Pro 1.7.5 (915) 30.09.2020, Advacam s.r.o., Prague, Czech Republic.
- [24] Krzyzanowska A. Measurements of charge sharing in a hybrid pixel photon counting CdTe detector, 2021 JINST 16 C12027. <https://doi.org/10.1088/1748-0221/16/12/C12027>.
- [25] Mathieson K, Passmore MS, Seller P, Prydderch ML, O'Shea V, Bates RL, et al. Charge sharing in silicon pixel detectors. Nucl Instrum Methods Phys Res A 2002; 487:113–22. [https://doi.org/10.1016/S0168-9002\(02\)00954-3](https://doi.org/10.1016/S0168-9002(02)00954-3).
- [26] Mathieson K, Bates R, O'Shea V, Passmore MS, Rahman M, Smith KM, et al. The simulation of charge sharing in semiconductor X-ray pixel detectors. Nucl Instrum Methods Phys Res A 2002;477:191–7. [https://doi.org/10.1016/S0168-9002\(01\)01894-0](https://doi.org/10.1016/S0168-9002(01)01894-0).
- [27] Myronakis ME, Darambara DG. Monte Carlo investigation of charge-transport effects on energy resolution and detection efficiency of pixelated CZT detectors for SPECT/PET applications. Med Phys 2011;38(1):455–67. <https://doi.org/10.1118/1.3532825>.
- [28] Goldman LW. Principles of CT: radiation dose and image quality. J Nucl Med Technol 2007;35(4):213–25. <https://doi.org/10.2967/jnmt.106.037846>.
- [29] Pellegrini G, Maiorino M, Blanchot G, Chmeissani M, Garcia J, Lozano M, et al. Direct charge sharing observation in single-photon-counting pixel detector. Nucl Instrum Methods Phys Res A 2007;573(1–2):137–40. <https://doi.org/10.1016/j.nima.2006.11.010>.
- [30] Bugby SL, Koch-Mehrini KA, Veale MC, Wilson MD, Lees JE. Energy-loss correction in charge sharing events for improved performance of pixellated compound semiconductors. Nucl Instrum Methods Phys Res A 2019;940:142–51. <https://doi.org/10.1016/j.nima.2019.06.017>.
- [31] Campbell M, Heijne E, Leroy C, Martin J-P, Mornacchi G, Nessi M, Pospisil S, Solc J, Soueid P, Suk M, Turecek D, Vykydal Z. Analysis of the Radiation Field in ATLAS Using 2008 2011 Data from the ATLAS-MPX Network, Tech. Rep., ATL-GEN-PUB-2013-001, CERN, Geneva, 2013.